Biosensors and Bioelectronics: X 23 (2025) 100595

Contents lists available at ScienceDirect

Biosensors and Bioelectronics: X

journal homepage: www.journals.elsevier.com/biosensors-and-bioelectronics-x

Characterization of plant pathogenic bacteria at subspecies level using a dielectrophoresis device combined with Raman spectroscopy

Alessio Sacco [a,*,1], Camilla Sacco Botto [b,1], Chiara D'Errico [b], Marina Ciuffo [b], Slavica Matić [b], Giulia Molinatto [c], Andrea M. Giovannozzi [a], Andrea M. Rossi [a], Emanuela Noris [b,**]

[a] Istituto Nazionale di Ricerca Metrologica, Strada delle Cacce 91, 10135, Torino, Italy
[b] Institute for Sustainable Plant Protection, National Research Council of Italy, Strada delle Cacce 73, 10135, Torino, Italy
[c] Phytosanitary Laboratory, Phytosanitary Sector and Technical-Scientific Services of the Piedmont Region, Via Livorno, 60, 10144, Torino, Italy

ARTICLE INFO

Keywords:
Raman spectroscopy
Dielectrophoresis
Machine learning
Plant pathogens
Diagnosis
Bacteria

ABSTRACT

Timely diagnosis of plant diseases and correct identification of etiological agents are fundamental to guarantee quality and quantity of agricultural products and food. Phytopathogenic bacteria induce devastating effects on crops. Their diagnosis and identification, mainly based on serological and molecular tools, are time consuming and expensive processes and require trained personnel. Among the innovative methods providing rapid, accurate, and reliable diagnosis at reduced costs, Raman spectroscopy (RS) is gathering considerable attention. RS provides a direct and non-destructive platform to gather information on the chemical and biochemical components of a sample, such as microorganism cultures, revealing their biological role. Due to the weak signals of bacterial cells in RS, a dielectrophoresis (DEP) approach was adopted to amplify the bacterial signals. Using Raman-DEP analysis, a dataset of spectra from different harmful phytopathogenic bacteria belonging to the genera *Pseudomonas* spp., *Xanthomonas* spp., and *Erwinia* spp. was obtained. Machine learning approaches were employed to discriminate isolates at the genus, species, and unprecedentedly at the pathovar level, reaching accuracies, precisions, recalls, and F1 scores of 94–100%. This approach offers important advancements in the non-destructive and rapid classification of microorganisms and is suitable to be readily extended to environmental and food diagnostics.

1. Introduction

Food availability and security are threatened by the incessant increase of the human world population, projected to reach over 9 billion by 2050, and by several agricultural issues linked to global warming. Among the latter, plant pests and diseases cause up to 40% of annual crop losses, undermining yield and quality of agricultural products (FAO, 2020; Savary et al., 2019; Baldi and La Porta, 2020). Furthermore, the increased trade of agricultural goods, foodstuffs, and reproductive plant materials promotes the spread of plant pathogens, namely bacteria, viruses, and fungi. These issues compel to increase the efforts to limit pathogen spread in order to guarantee food security and support the sustainability of food sources. In this context, it is fundamental to achieve accurate and timely detection and identification of pathogens, to limit the progression of new or already existing diseases and prevent the entry of quarantine pathogens into new geographical areas.

Typically, diagnosis and identification of plant pathogens rely on symptom evaluation, feasible only when tissue or organ alterations are already evident or, alternatively with microscopic, serological, biochemical, physiological, or molecular techniques (Venbrux et al., 2023), characterized by different levels of sensitivity and technical complexity. For culturable bacteria, these procedures involve the extraction of proteins or nucleic acids employed for serological or molecular identification. However, these procedures require at least 3–5 days to be accomplished and, in case of nucleic acid detection methods, further time for sequencing and sequence analyses should be added. As these activities are time consuming, expensive, and require trained personnel, new and innovative detection methods are sought, aimed at shortening and simplifying the process, meanwhile preserving accuracy, reliability, and sustainability (Fang and Ramasamy, 2015; Baldi and La

* Corresponding author.
** Corresponding author.
E-mail addresses: a.sacco@inrim.it (A. Sacco), emanuela.noris@ipsp.cnr.it (E. Noris).
[1] These authors contributed equally in this work.

https://doi.org/10.1016/j.biosx.2025.100595
Received 9 October 2024; Received in revised form 17 January 2025; Accepted 12 February 2025
Available online 20 February 2025

Porta, 2020; Venbrux et al., 2023).

Recently, optical spectroscopy and imaging techniques have been proposed as innovative strategies in agricultural diagnostics. These approaches include Raman spectroscopy (RS) as a direct label-free detection platform to rapidly analyze the whole chemical composition of a biological matrix. RS measures the wavelength differences in scattered light linked to vibration energy levels of chemical bonds after their excitation (Tu and Chang, 2012). Among the various applications, RS has been implemented for the detection and classification of bacteria (Huang et al., 2010; Lu et al., 2011; Kusić et al., 2015; Rebrošová et al., 2017; Stöckel et al., 2016; Ho et al., 2019; de Siqueira e Oliveira et al., 2020; Bräuer et al., 2022; Cui et al., 2022; Lorenz et al., 2022; Thomsen et al., 2022; PM 7/20 Erwinia amylovora, 2022; Rebrosova et al., 2022; Dragounová et al., 2023; Ogunlade et al., 2024). However, the low Raman cross-section of bacterial cells (Rodriguez et al., 2023) imposes to explore strategies that amplify the Raman signal intensity. Here, a device based on dielectrophoresis (DEP) has been used as a particle manipulation technique operating in liquid conditions, useful to concentrate bacterial cells in the focal volume of a Raman microscope and to amplify the intensity of the spectroscopic signal, as we previously showed with human pathogenic bacteria (Barzan et al., 2020, 2022).

In the present work, we applied a combined Raman-DEP approach to obtain a dataset of Raman spectra from phytopathogenic bacteria, implementing deep learning methods to accurately identify the pathogens. Starting from the "Top-10 list" of phytopathogenic bacteria (Mansfield et al., 2012), isolates belonging to the most important genera *Pseudomonas*, *Xanthomonas*, and *Erwinia* were included, concentrating on a few species whose spread in Europe is supervised by the European Food Safety Authority (EFSA). Noteworthy, some of the organisms considered in this work, i.e. *Xanthomonas axonopodis* pathovar (pv.) *phaseoli*, *Pseudomonas syringae* pv. *actinidiae*, and *Erwinia amylovora* are quarantine bacteria, recognized in the A2 list drawn up by the European and Mediterranean Plant Protection Organization (EPPO) (https://www.eppo.int/ACTIVITIES/plant_quarantine/A2_list). More specifically, *P. syringae* pv. *actinidiae* is a harmful pathogen responsible for the bacterial canker of kiwifruit trees which, together with the Kiwifruit vine decline syndrome, concurs to determine heavy yield losses in kiwifruit plantations (Scortichini et al., 2012; Vanneste, 2017). The list also comprised isolates of *E. amylovora*, causing the fire blight disease of rosaceous fruit plants (such as apple, pear, and quince) and affecting various ornamental plants (Fire Blight, 2000; Kałużna et al., 2016). As climate change favors the spread of this disease, more frequent and stringent phytosanitary controls are necessary, specifically on vegetatively propagated material (dormant buds and scions) which represent long-term survival sites for this pathogen (EPPO Bulletin, 2022). Besides, two harmful pathogens of bean, i.e. *P. syringae* pv. *phaseolicola,* responsible for the halo blight disease, causing up to 43% of crop losses (Prosen et al., 1993) and *X. axonopodis* pv. *phaseoli*, inducing the brown spot disease were also considered in this study, with the intent of discriminating different pathogens affecting the same crop. Due to the deep classification of certain bacterial species into pathovars, machine learning techniques were applied to maximize the discrimination potential.

Overall, the Raman-DEP method adopted allowed us to reach high levels of accuracy in the distinction of bacteria at the genus, species, and even pathovar level, and can be proposed as a successful strategy for discriminating and identifying bacteria of different living environments.

2. Materials and Methods

2.1. Dataset description

The reference dataset used in this study consisted of 39 Gram-negative bacteria, including multiple isolates belonging to three different genera (*Pseudomonas*, *Xanthomonas*, and *Erwinia*) and 11 different taxonomic groups. The detailed list of the isolates is provided in Table 1. For each genus, two bacterial species were included, i.e. (a) *P. syringae* and *P. marginalis*, (b) *X. arboricola* and *X. axonopodis*, and (c) *E. amylovora* and *E. herbicola*. *P. marginalis*, *E. amylovora*, and *E. herbicola* were represented at the species level, while for the other species pathovars were also included, i.e. (a) four pathovars for *P. syringae* (*phaseolicola, actinidiae, morsprunorum*, and *syringae*), (b) two for *X. arboricola* (*corylina* and *juglandis*), (c) and one for *X. axonopodis* (*phaseoli*). All bacterial isolates were identified using Polymerase Chain Reaction (PCR), according to the EPPO guidelines (see Table 1 for details).

2.2. Characterization of bacterial isolates using the DEP-Raman device

For each isolate, a single colony was picked from a fresh agar plate and inoculated into 5 ml of low salt Luria broth (LS-LB) (tryptone, 10 g; NaCl, 5 g; yeast extract, 5 g/l deionized water) and cultured overnight at 26 °C with shaking at 180 rpm. Following centrifugation (6000 rpm, 10 min, 4 °C), the bacterial pellet was washed three times with phosphate-buffered saline (PBS) solution and resuspended in 0.5 × PBS, until OD_{600} of 0.3 was reached.

The DEP cell coupled to the Raman microscope was as previously described (Barzan et al., 2020), with slight modifications. Briefly, the DEP cell consisted of a chamber formed by poly-tetrafluoroethylene (PTFE) lateral walls and a glass coverslip top, through which the sample was analyzed. The bottom of the cell was an active glass chip with a quadrupole of gold electrodes, in the middle of which the lowest electric field density was reached. Electrodes were biased with alternate voltage of 1 MHz frequency and 5 V peak-to-peak amplitude. After voltage application, the resulting negative DEP forces induced agglomeration of bacterial cells in the middle of the chip below the confocal volume in less than 15 s, saturating the Raman spectral amplitudes. To avoid sampling biases and to multiply the number of cells analyzed, for each sample, different aliquots were injected in the DEP cell, and analyzed separately.

Bacterial cells were observed using a DXR™ Raman confocal microscope (Thermo Scientific) in a 180° backscattering configuration, equipped with an excitation laser (532 nm wavelength, 20 mW power) for a total exposure time of 1 min per spectrum. Each spectrum consisted of 60 averaged acquisitions of 1 s each. For each aliquot, at least five spectra were acquired. Spectra were gathered with the dispersive Raman system having a mean spectral resolution of 5 cm^{-1} in the range of 3100–500 cm^{-1}, collecting 3489 points per spectrum. A 60 × water immersion microscope objective with a numerical aperture of 1.1 (Olympus LUMFLN-W) was used. In these conditions, the lateral resolution of the microscope was estimated to be approximately 0.5 μm, while the collection of the confocal volume of the Raman microscope accounted to approximately 3.0 μm^3 (Sacco et al., 2021). Spectral calibration of the Raman microscope was performed before each measurement session to guarantee reproducibility; for this, the emission wavelengths of a neon lamp were measured and compared to tabulated data for spectral frequency (Raman shift); in addition, the fluorescence spectrum of a traceable artifact (ASTM E1840-96, 2014) stimulated by the excitation laser for spectral intensity was acquired (Satterfield et al., 2008). Spectra were obtained in several measuring sessions to take into consideration potential instrumental variability. In particular, four different experiments were conducted; in each experiment, a representative set of the isolates was analyzed, including every time a biological replicate of a previously tested isolate, to prevent possible batch effects.

2.3. Data analysis and multivariate modeling

Before multivariate analysis, spectra were subjected to a preprocessing step. First, the data were cropped to a wavenumber range of [700; 1750] cm^{-1}, focusing the model on the "fingerprint" spectral region. Then, a smoothing step was performed on each spectrum with second order Savinsky-Golay filtering, using a 11-points window. Multiplicative scatter correction (MSC) was then utilized to uniform the

Table 1
List of bacterial isolates used in the present study.

Genus	species	pathovar	Geographical origin	Plant of isolation	Tissue	Genotyping
Pseudomonas	*syringae*	*phaseolicola*	Piedmont, Italy	*Phaseolus vulgaris*	leaf	Audy et al., 1996; Prosen et al. (1993)
			Piedmont, Italy	*Phaseolus vulgaris*	leaf	
			Piedmont, Italy	*Phaseolus vulgaris*	leaf	
			Piedmont, Italy[a]	*Phaseolus vulgaris*	leaf	
			China[a]	*Phaseolus vulgaris*	seed	
Pseudomonas	*syringae*	*actinidiae*	Piedmont, Italy	*Pyrus communis*	stem	Gallelli et al. (2011); Koh and Nou (2002)
			Piedmont, Italy	*Actinidia chinensis*	leaf	
			Piedmont, Italy	*Actinidia chinensis*	leaf	
			Veneto, Italy	*Actinidia chinensis*	leaf	
			Veneto, Italy	*Actinidia chinensis*	leaf	
			Piedmont, Italy	*Actinidia chinensis*	necrotic branch	Rees-George et al. (2010)
Pseudomonas	*syringae*	*morsprunorum*	Piedmont, Italy	*Prunus avium*	leaf	Kaluzna et al., 2016
			Piedmont, Italy	*Prunus avium*	stem	
			Worcestershire, UK	*Prunus avium*	leaf	Plant Health Solutions Ltd
			Worcestershire, UK	*Prunus avium*	leaf	
			W. Sussex, UK	*Prunus avium*	leaf	
			Oxfordshire, UK	*Prunus avium*	leaf	
			W. Sussex, UK	*Prunus domestica*	leaf	
			Worcestershire, UK	*Prunus domestica*	leaf	
Pseudomonas	*syringae*	*syringae*	Piedmont, Italy[a]	*Pyrus communis*	stem	Sorensen et al. (1998)
			Piedmont, Italy	*Prunus armeniaca*	branch	
			Warwickshire, UK	*Prunus* sp.	shoot	Plant Health Solutions Ltd
			Worcestershire, UK	*Prunus avium*	leaf	
			W. Sussex, UK	*Prunus avium*	leaf	
			Worcestershire, UK	*Prunus domestica*	leaf	
			Worcestershire, UK	*Prunus domestica*	leaf	
Pseudomonas	*marginalis*	-	Piedmont, Italy	*Lactuca sativa*	leaf	Ravatn et al. (1998); Lane (1991)
			Piedmont, Italy	*Lactuca sativa*	leaf	
Xanthomonas	*arboricola*	*corylina*	Piedmont, Italy	*Corylus avellana*	stem	Lane (1991)
Xanthomonas	*arboricola*	*juglandis*	Piedmont, Italy	*Juglans regia*	leaf	Mbega et al. (2012)
Xanthomonas	*axonopodis*	*phaseoli*	Hungary	*Phaseolus vulgaris*	N/A	Ravatn et al. (1998)
Erwinia	*amylovora*	-	Piedmont, Italy	*Malus domestica*	stem	EPPO PM7/20(3) Appendix 9
			Piedmont, Italy	*Pyrus communis*	stem	
Erwinia	*herbicola*	-	Piedmont, Italy	*Corylus avellana*	branch	Audy et al., 1994; Ravatn et al. (1998)

[a] This isolate was tested in two different experiments.

dataset (Geladi et al., 1985), followed by baseline correction by asymmetric least squares smoothing on each spectrum (Eilers and Boelens, 2005), with $p = 10^{-2}$ asymmetry and $\lambda = 10^5$ smoothness parameters. Data were then normalized (l2 normalization) and mean centered. Standardization (i.e. rescaling variables to unit variance) was not applied to preserve the useful information on intensities, since these are directly proportional to the amount of substance in the bacteria.

Multivariate analysis was performed with the scikit-learn Python library (Pedregosa et al., 2011). Classification was achieved by treating the data with dimensionality reduction by partial least squares (PLS, a.k.a. projection to latent structures) (Wold et al., 2001) before using the support vector machine (SVM) technique for classification (Cortes and Vapnik, 1995). PLS was utilized only for decomposition to a more compact set of variables, without the regression or classification step usually performed after this (i.e. PLS regression or PLS discriminant analysis).

After preprocessing and before PLS-SVM, the dataset was split into a training set and a test set. The training set was used to construct the models, evaluate their performances with different approaches and establish the hyperparameters resulting from each of the models. Models with optimized parameters were then applied to the test set of data, consisting in all cases, of 20% of the total dataset. Test data in this phase was extracted from the total dataset proportionally from each class and isolate (in a process also known as stratification). One hundred rounds of randomly-folded 5-fold cross validation were averaged to calculate the performance in the training phase. The output of these analyses was obtained based on several commonly employed metrics during the training and after the test step, i.e. accuracy, precision, recall, and F1 score (Powers, 2008).

In order to test the robustness of the model in a stricter way, an identification step was also performed on the dataset. Identification was done on spectra taken on independent isolates: this was achieved in this work by excluding an isolate of each pathovar from the starting dataset — based on acquisition date and number of spectra — so that a model could built on approximately 80% of the dataset, and use strains not included in model construction (training/identification data points ratio ~4:1).

3. Results and discussion

3.1. Dataset acquisition

The Raman dataset considered in this work consisted of 5–15 spectral acquisitions for each of the bacterial isolates. Overall, 34 isolates of *Pseudomonas*, three of *Xanthomonas,* and two of *Erwinia* were analyzed, forming a dataset of 323 spectra (Table 1).

3.2. Model construction

The construction of the model aimed at maximizing the classification results with the least amount of model complexity and degrees of freedom, testing the validity of the Raman-DEP discrimination approach at different taxonomic levels, and producing models with the highest level of robustness, as complex models are usually more prone to overfitting. The three models described differ in the number of PLS variables (latent variables, henceforth named LVs in the text) and in the functions used in the SVM kernels. Models were considered less complex as the number of LVs employed was lower, and a linear kernel function was less prone to overfitting than a radial basis function (rbf).

The hyperparameters of the final preprocessing pipeline and the models were selected maximizing accuracy, precision, recall, and F1 score in the training phase. A balance in the metrics was sought in the validation step before applying the models to the test data, although there was no particular trend leading to clearly distinguishing the

models.

3.3. Classification at the genus level

The first goal of this research was to evaluate the performances of the Raman-DEP procedure in the discrimination of phytopathogenic bacteria belonging to different genera. Specific signals obtained with the Raman-DEP device were considered, selecting the molecular fingerprint region between 700 and 1750 cm^{-1}. The mean spectra obtained differed between the isolates based on their genera and, in particular, isolates classified as *Erwinia* spp. had the most distinctive pattern (Fig. 1a). The different patterns obtained were related to the chemical assignments of the bands of the most distinctive peaks for each genus, such as C-N, tyrosine, and s ν2(C-C; carotenoids) signals (Table 2).

More specifically, as shown in Fig. 1a, the spectra could be distinguished based on the relative intensities of all the most significant bands, included but not limited to the most Raman active peaks corresponding to amino acids, lipids, DNA, cytochrome, and carotenoids. In particular, the averaged Raman spectrum of *Erwinia* isolates is characterized by very pronounced carotenoids peaks (1526 cm^{-1}, 1157 cm^{-1}), which appear less intense and only barely visible in the spectra of *Xanthomonas* and *Pseudomonas*, respectively. On the other side, the averaged spectrum of *Xanthomonas* isolates is characterized by a strong C-N, cytosine, uracil peak (1128 cm^{-1}), which is also evident in the case of *Pseudomonas*, but appears weak in the spectrum of *Erwinia*. Furthermore, the cytochrome peak (748 cm^{-1}), which is fairly intense in the spectra of *Xanthomonas* and *Pseudomonas*, is only barely visible in the case of *Erwinia*. Conversely, the averaged spectrum of *Pseudomonas* is characterized by several additional important peaks, such as DNA (783 cm^{-1}), phenylalanine (1003 cm^{-1}), amide III (1233 cm^{-1}), cytosine, adenine, uracil, (1306 cm^{-1}), δ_{CH}, tryptophan, adenine, guanine (1337 cm^{-1}), δ_{CH2} (lipids) (1454 cm^{-1}), m δ(CH2) and δ(CH3) (1481 cm^{-1}), adenine, guanine (1580 cm^{-1}) and amide I (1659 cm^{-1}). To evaluate if isolates belonging to the same genus could be distinguished based on Raman spectra analysis, a PLS-SVM classification method was used. Simpler methods would also be appropriate, but the PLS-SVM classification method was already applied in other, finer classifications. Specifically, a three class model (*Pseudomonas*, *Erwinia*, and *Xanthomonas)* SVM linear kernel with three LVs was applied. The score plots of the PLS model in the area defined by the LVs are shown in Fig. 1b, providing a clear indication of the specificity and sensitivity of the model. The classification results of the cross-validation test indicate that the model allows the classification of the spectra at the genus level, with 100% accuracy and 100% precision (Table 3).

3.4. Classification at the species level

Furthermore, we intended to evaluate if the procedure could discriminate between bacterial isolates belonging to different species within the same genus. The analysis was conducted on isolates of *Pseudomonas*, selected as it included the most abundant number of isolates in our list. The average spectra for two *Pseudomonas* species are depicted in Fig. 2a. In this case, the differences between the groups are less evident, but it is still possible to discern discrepancies in some bands ratios, such as those associated to tryptophan and amides compared to those associated to DNA. In particular, the averaged Raman spectrum of *P. marginalis* is characterized by a strongly pronounced cytochromepeak (747 cm^{-1}), higher than the corresponding peak in the *P. syringae* spectrum. Conversely, the *P. syringae* spectrum is characterized by larger peaks of DNA (783 cm^{-1}), Phenylalanine and carotenoids (1003 cm^{-1}), C-N, P (1098 cm^{-1}), amide III (1233 cm^{-1}), C, A, U (1306 cm^{-1}), δCH, Trp, A, G (1337 cm^{-1}), δCH2(Lipids) (1454 cm^{-1}), m δ(CH2) and δ(CH3) (1481 cm^{-1}) and amide I (1659 cm^{-1}). Noteworthy, the main inter species differences are the dominant source of the intra genus

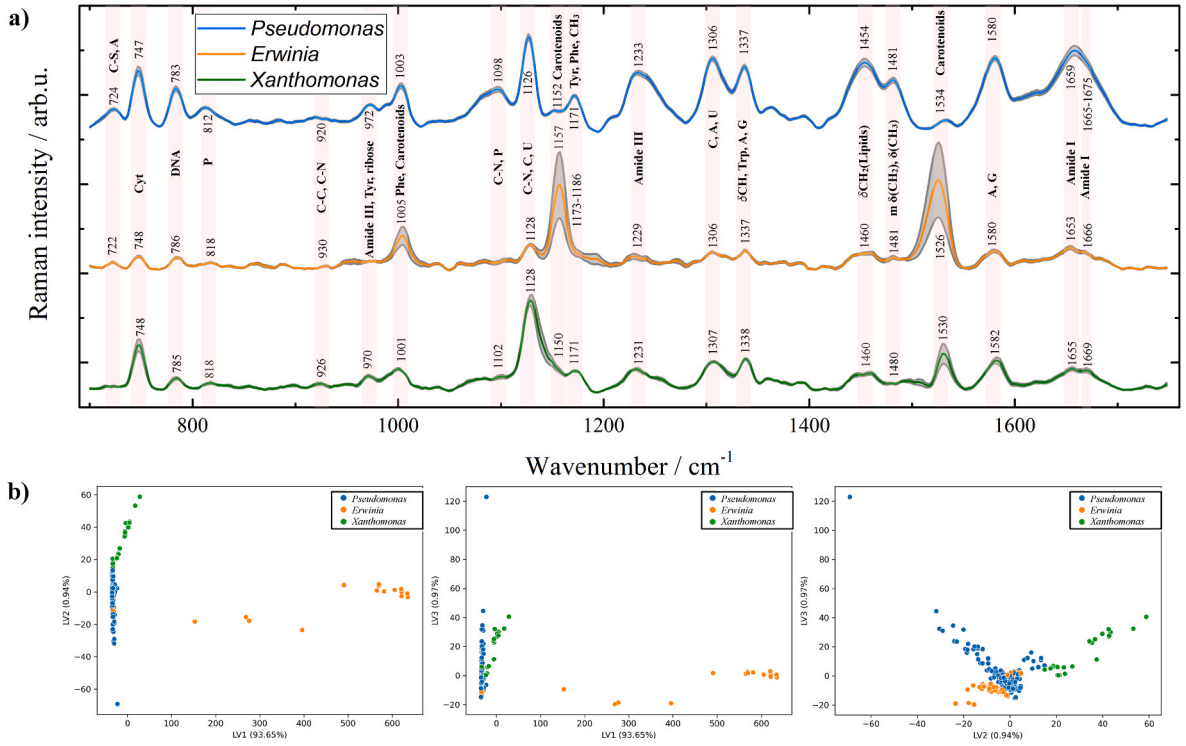

Fig. 1. Raman spectra of phytopathogenic bacteria belonging to the three genera *Pseudomonas*, *Erwinia*, and *Xanthomonas*. a) Average Raman spectra of the isolates classified as *Pseudomonas* (245 acquisitions, blue), *Erwinia* (51 acquisitions, orange), and *Xanthomonas* (30 acquisitions, green), normalized to the maximum at 1126 cm^{-1}, 1526 cm^{-1}, and 1128 cm^{-1}, respectively. Spectra were preprocessed as detailed in the Materials and Methods section. The grey areas depict the variations of the measured spectra (mean ± 1.96 × standard error of the mean). **b)** Classification by PLS-SVM model with three latent variables. (For interpretation of the references to colour in this figure legend, the reader is referred to the Web version of this article.)

Table 2
Raman band assignment for phytopathogenic bacteria.

Assignment	*Pseudomonas* spp.	*Erwinia* spp.	*Xanthomonas* spp.	Reference
Amide I	1665–75	1666	1669	1669 (Turano et al., 1976);
Amide I	1659	1653	1655	1660 (Deng et al., 1993);
A, G	1580	1580	1582	1580 (Manoharan et al., 1990), 1575–1580 (Lorenz et al., 2022);
s ν1(C=C) (Carotenoids)	1534	1526	1530	1153–1157 (Lorenz et al., 2017);
m $\delta(CH_2)$ and $\delta(CH_3)$	1481	1481	1480	1483 (Mansfield et al., 2012, Manoharan et al., 1990);
δCH_2 (Lipids)	1454	1460	1460	1458 (Turano et al., 1976);
δCH, Trp, A, G	1337	1337	1338	1333-1331-1337-1338-1339 (Cialla et al., 2009; Turano et al., 1976);
C, A, U	1306	1306	1307	1296-1305 (Turano et al., 1976);
Amide III	1233	1229	1231	1230-1300 (Ruokola et al., 2014; Turano et al., 1976);
Tyr, Phe, CH_3	1171	1173–1186	1171	1178 (Turano et al., 1976); 1156–1176 (Reilly and Thomas, 1994);
s ν2(C-C) (Carotenoids)	1152	1157	1150	1500–1550 (Lorenz et al., 2017);
C-N, C, U	1126	1128	1128	1127 (Turano et al., 1976), 1125 (Deng et al., 1993);
C-N, P	1098	–	1102	1100 (Turano et al., 1976), 1091 (Ruokola et al., 2014);
Phe and C-CH_3 (Carotenoids)	1003	1005	1001	1000-1005 (Turano et al., 1976), 1003 (Ruokola et al., 2014), 1004 (Lorenz et al., 2017), 1004 (Lorenz et al., 2019);
Amide III, Tyr, ribose	972	–	970	960-978 (Ruokola et al., 2014), 971 (Cialla et al., 2009), 982 (Deng et al., 1993);
C-C, C-N	920	930	926	938 (Turano et al., 1976), 931 (Cialla et al., 2009), 932 (Deng et al., 1993);
P	812	818	818	812 (Turano et al., 1976), 811 (Ruokola et al., 2014);
C, U, T, Trp, His, Thr	783	786	785	785 (Turano et al., 1976), 771 (Cialla et al., 2009),770 (Deng et al., 1993), 783 (Ruokola et al., 2014);
cyts	747	748	748	747 (Lorenz et al., 2019), 748 (Lorenz et al., 2022);
C-S, A	724	722	–	723-726 (Turano et al., 1976);

Table 3
PLS-SVM classification to distinguish bacterial isolates at the genus level. Confusion matrix of a) training data and b) test data.

a)

Training data		Actual values		
		Pseudomonas	Erwinia	Xanthomonas
Predicted values	*Pseudomonas*	195	0	0
	Erwinia	0	41	0
	Xanthomonas	0	0	24

b)

Test data		Actual values		
		Pseudomonas	Erwinia	Xanthomonas
Predicted values	*Pseudomonas*	50	0	0
	Erwinia	0	10	0
	Xanthomonas	0	0	6

variance in the averaged spectrum of the *Pseudomonas* (Fig. 1).

At the same time, in the comparison between species, a PLS-SVM classification method, with a two class model (*P. syringae* and *P. marginalis)* SVM linear kernel after a two LVs PLS dimensionality reduction was applied. The score plots of the PLS model in the area defined by the LVs are represented in Fig. 2b. As shown in the classification results of the cross-validation test, the model allowed to classify *Pseudomonas* isolates at the species level, with 100% accuracy and 100% precision (Table 4).

3.5. Classification at the pathovar level

The most ambitious goal of this work was to discriminate isolates belonging to different pathovars, within the same species. For this, we focused on isolates classified as *P. syringae* belonging to four different pathovars. Fig. 3a shows the mean spectra obtained from all the acquisitions of the available isolates. In this case, it was not possible to rely on signal ratios or peak positions to discriminate the classes when spectral variability is taken into consideration, and machine learning approach was necessary.

Following evaluation of the spectra with a PLS-SVM classification method, a four class model (*P. syringae* pv. *morsprunorum*, *P. syringae* pv. *actinidiae*, *P. syringae* pv. *phaseolicola*, and *P. syringae* pv. *syringae)* SVM

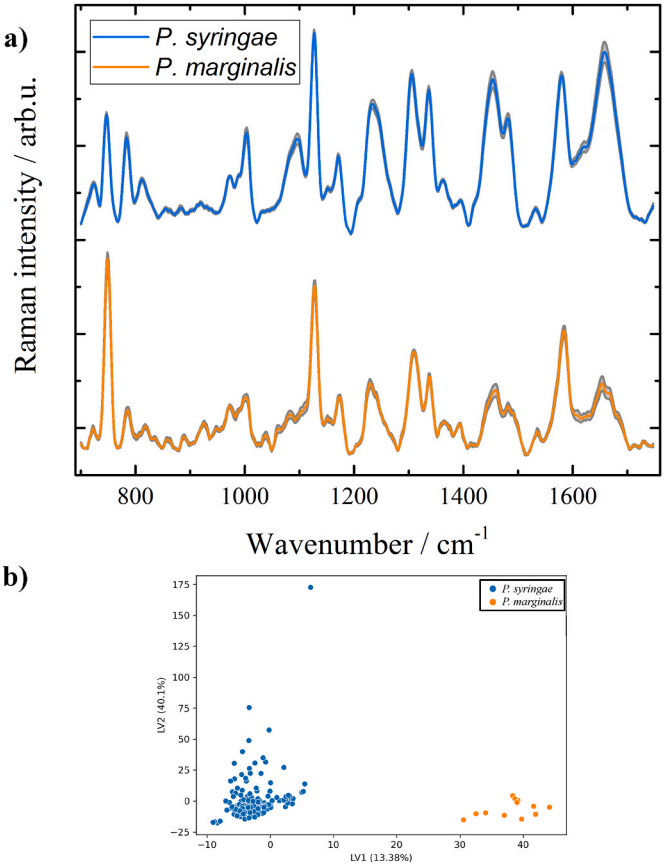

Fig. 2. Raman-DEP spectra of phytopathogenic bacteria belonging to the two species of the *Pseudomonas* genus, i.e. *P. syringae* and *P. marginalis*. a) Average Raman spectra of 230 acquisitions of *P. syringae* (blue) and 15 of *P. marginalis* (green), normalized to the maximum at 1126 cm^{-1}, and 749 cm^{-1}, respectively. Spectra were pre-processed as described in Materials and Methods. The grey areas depict the variations of the spectra (average ± 1.96 × sem). b) Classification by PLS-SVM model with two latent variables. (For interpretation of the references to colour in this figure legend, the reader is referred to the Web version of this article.)

Table 4
PLS-SVM classification to distinguish bacterial species within the genus *Pseudomonas*. Confusion matrix of a) training data and b) test data.

a)

Training data		Actual values	
		P. syringae	P. marginalis
Predicted values	*P. syringae*	184	0
	P. marginalis	0	12

b)

Test data		Actual values	
		P. syringae	P. marginalis
Predicted values	*P. syringae*	46	0
	P. marginalis	0	3

with a radial basis function (rbf) kernel, on a PLS-reduced dataset with three LVs was applied. The score plots of the PLS-SVM model in the area defined by the LVs are shown in Fig. 3b. In this case, the classification results of the cross-validation test showed that the model could classify isolates at the pathovars level with 93% accuracy, 95% precision, and 96% recall (F1 score: 95%) on external data with most outliers being *P.s.* pv. *syringae* erroneously classified as pv. *morsprunorum* (Table 5). The genus *Pseudomonas* is the largest genus of Gram-negative bacteria and, in particular, the *P. syringae* species complex includes several species taxonomically closely related (Bull et al., 2010). The inaccurate classification of *P.s.* pv. *morsprunorum* and pv. *syringae* could be associated with their closer chemical affinity, possibly linked to their pathogenicity, in fact, as both these pathovars induce the bacterial canker of sweet cherry (*Prunus avium*) (Bultreys and Kaluzna, 2010). Although the *Pseudomonas* classification is continuously revisited thanks to new genome sequence analysis (Gomila et al., 2017, Lalucat et al., 2022), the procedure described in this study adds different elements useful for rapid and economic diagnostic classification of these pathogens.

The robustness of the method was then further verified for pathovars in a validation step. This was performed by training a model with the same multivariate techniques, hyperparameters and spectral preprocessing pipeline, but in this case excluding one isolate for each pathovar for training, effectively constructing an independent verification dataset of similar size to the previous test set. The results are comparable to the ones from the test phase, and are shown in Table 6: the model classified the four pathovars in the verification dataset with 95% accuracy, 96% precision, and 94% recall, hence a F1 score equal to 95%.

A summary of the results of the classification models to distinguish genus, species and pathovar is shown in Table 7.

4. Conclusions

Bacterial identification most commonly relies on the use of conventional microbiological methods consisting in the cultivation on specific culture media, followed by morphological, physiological, and biochemical tests or on the use of molecular approaches, mainly based on PCR or its modifications, followed by sequencing (Franco-Duarte et al., 2019). Different approaches relying on mass spectrometry, such as MALDI-TOF MS (Ashfaq et al., 2022) and electrospray ionization (ESI)-MS (Sampath et al., 2007) and RS (Stöckel et al., 2016; Cui et al., 2022) are also under investigation for rapid and low labor applications

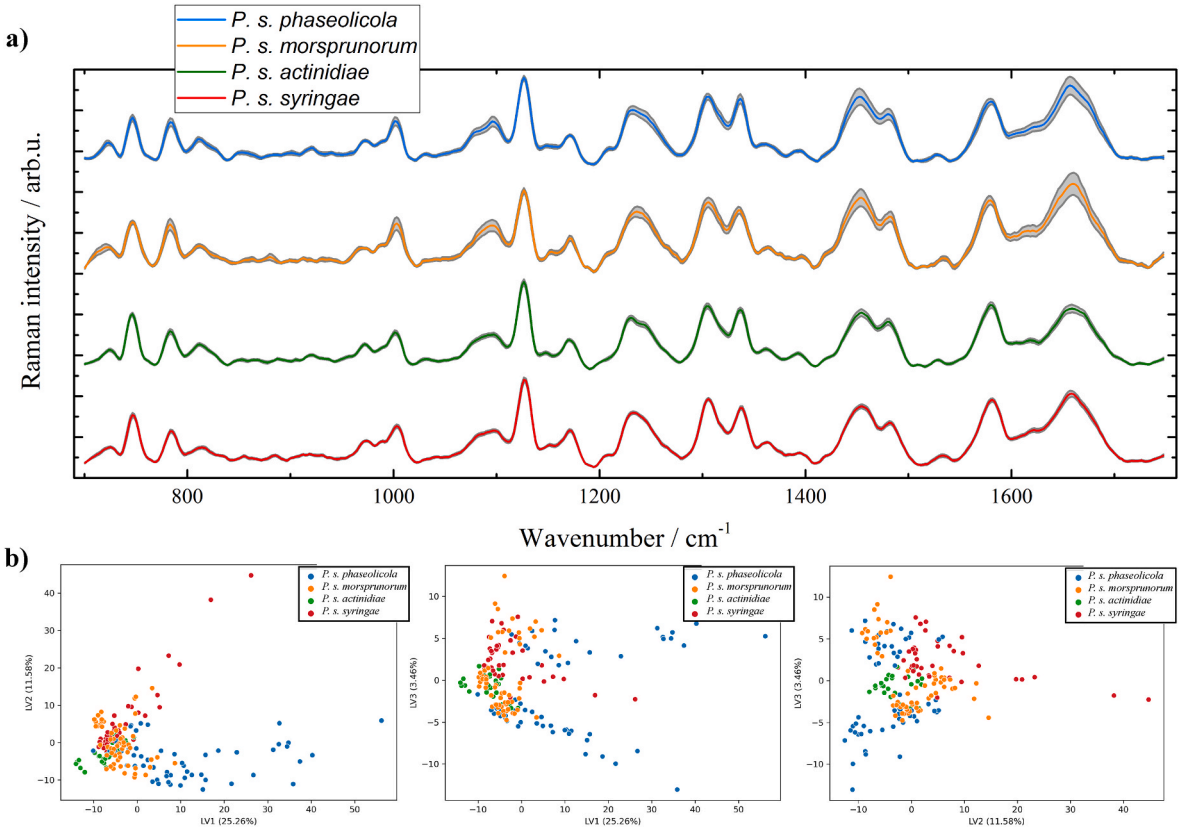

Fig. 3. Raman-DEP spectra of *Pseudomonas syringae* isolates of different pathovars. **a)** Average Raman spectra of 66 acquisitions of *P. s.* pv. *morsprunorum* (blue), 31 acquisitions of *P. s.* pv. *actinidiae* (orange), 45 acquisitions of *P. s.* pv. *phaseolicola* (green), and 88 acquisitions of *P. s.* pv. *syringae* (red), normalized to the maximum at 1661 cm^{-1} for *P. s.* pv. *morsprunorum*, and 1126 cm^{-1} for *P. s.* pv. *actinidiae*, *P. s.* pv. *phaseolicola*, and *P. s.* pv. *syringae*. Spectra were preprocessed (see Materials and Methods). The grey areas depict the variations of the measured spectra (mean ± 1.96 × sem). **b)** Classification by PLS-SVM model with three latent variables. (For interpretation of the references to colour in this figure legend, the reader is referred to the Web version of this article.)

Table 5
PLS-SVM classification to distinguish bacterial pathovar of *Pseudomonas syringae* in the test step. Confusion matrix of a) training data and b) test data.

a)					
Training data		Actual values			
		P. s. pv. *morsprunorum*	*P. s.* pv. *actinidiae*	*P. s.* pv. *phaseolicola*	*P. s.* pv. *syringae*
Predicted values	*P. s.* pv. *morsprunorum*	43	0	0	10
	P. s. pv. *actinidiae*	0	25	0	0
	P. s. pv. *phaseolicola*	1	0	35	0
	P. s. pv. *syringae*	0	0	0	70
b)					
Test data		Actual values			
		P. s. pv. *morsprunorum*	*P. s.* pv. *actinidiae*	*P. s.* pv. *phaseolicola*	*P. s.* pv. *syringae*
Predicted values	*P. s.* pv. *morsprunorum*	13	0	0	3
	P. s. pv. *actinidiae*	0	6	0	0
	P. s. pv. *phaseolicola*	0	0	9	0
	P. s. pv. *syringae*	0	0	0	15

Table 6
PLS-SVM classification to distinguish bacterial pathovar of *Pseudomonas syringae* in the external verification step. Confusion matrix of a) training data and b) test data.

a)					
Training data		Actual values			
		P. s. pv. *morsprunorum*	*P. s.* pv. *actinidiae*	*P. s.* pv. *phaseolicola*	*P. s.* pv. *syringae*
Predicted values	*P. s.* pv. *morsprunorum*	48	0	0	10
	P. s. pv. *actinidiae*	0	25	0	0
	P. s. pv. *phaseolicola*	1	1	35	0
	P. s. pv. *syringae*	1	0	0	70
b)					
Test data		Actual values			
		P. s. pv. *morsprunorum*	*P. s.* pv. *actinidiae*	*P. s.* pv. *phaseolicola*	*P. s.* pv. *syringae*
Predicted values	*P. s.* pv. *morsprunorum*	5	0	1	1
	P. s. pv. *actinidiae*	0	6	0	0
	P. s. pv. *phaseolicola*	2	0	7	0
	P. s. pv. *syringae*	0	0	0	17

Table 7
PLS-SVM classification to distinguish bacterial isolates based on genus, species or pathovar.

		Accuracy	Precision	Recall	F1 Score
Genera (3)	Training data	100	100	100	100
	Test data	100	100	100	100
Species (2)	Training data	100	100	100	100
	Test data	100	100	100	100
Pathovars (4)	Training data	94	96	95	95
Test step	Test data	93	95	96	95
Pathovars (4)	Training data	92	94	93	93
Verification	Verification	95	96	94	95
step	data				

in diagnostic assays technologies.

The RS-based procedure developed in this study allowed to minimize the sample handling steps and reduce the processing time, thus avoiding nucleic acid extraction procedures and the use of sequencing services or in alternative avoid the extraction of proteins and the use of serological reagents. To increase the sensitivity of RS, a confocal Raman microscope was combined to a DEP cell permitting a successful discrimination of phytopathogenic bacteria at the pathovar level. This label-free technique allowed to elucidate the chemical composition (nucleic acids, proteins, lipids, pigments, and carbohydrates) of pure bacterial cultures, using a minimal amount of sample in a single measurement.

We demonstrate that it is possible to discriminate at the genus and species level dangerous bacterial pathogens affecting high value crops with accuracy and precision greater than 93%, indicating that Raman-DEP is a promising approach for a faster diagnosis of plant pathogenic bacteria. Moreover, within the *P. syringae* complex, which includes more than 60 pathovars (Bull et al., 2010), each one infecting a specific group of host plants, we succeeded to differentiate isolates belonging to four different pathovars, with accuracy, precision and recall greater than 94%.

For a wider application of this technique in plant pathology, larger datasets including bacterial isolates with diverse pathogenicity features, higher genetic diversity, differential susceptibility to antibiotics or bacteriophages, and different growth conditions would be needed.

CRediT authorship contribution statement

Alessio Sacco: Writing – original draft, Methodology, Investigation, Formal analysis, Conceptualization. **Camilla Sacco Botto:** Methodology, Investigation, Formal analysis. **Chiara D'Errico:** Writing – review & editing, Writing – original draft, Methodology, Investigation, Formal analysis. **Marina Ciuffo:** Methodology, Investigation. **Slavica Matić:** Methodology, Investigation. **Giulia Molinatto:** Investigation. **Andrea M. Giovannozzi:** Supervision, Funding acquisition. **Andrea M. Rossi:** Writing – review & editing, Funding acquisition, Conceptualization. **Emanuela Noris:** Writing – review & editing, Supervision, Funding acquisition, Conceptualization.

Declaration of competing interest

The authors declare that they have no known competing financial

interests or personal relationships that could have appeared to influence the work reported in this paper.

Acknowledgements

This research was funded by Fondazione Cassa di Risparmio di Torino, Project BatRam: Diagnosis of phytopathogenic bacteria by means of Raman spectroscopy and machine learning, N. 2022.AI590.U709. (2) "Agritech National Research Center" funded by the European Union Next-GenerationEU (PIANO NAZIONALE DI RIPRESA E RESILIENZA (PNRR) – MISSIONE 4 COMPONENTE 2, INVESTIMENTO 1.4 – D.D. 1032 June 17, 2022, CN00000022), (3) "ON Foods - Research and innovation network on food and nutrition Sustainability, Safety and Security – Working ON Foods" (code PE00000003) within the National Recovery and Resilience Plan (NRRP) Mission 4 Component 2 Investment 1.3 - Call for proposals No. 341 of March 15, 2022 of Italian Ministry of University and Research (MUR), funded by the European Union – NextGenerationEU. (4) Italian Ministry of University and Research (MUR) in the framework of the continuing-nature project "NEXT- GENERATION METROLOGY", under the allocation of the Ordinary Fund for research institutions (FOE) 2023 (Ministry Decree n. 789/2023).

Data availability

Data will be made available on request.

References

Ashfaq, M.Y., Da'na, D.A., Al-Ghouti, M.A., 2022. Application of MALDI-TOF MS for identification of environmental bacteria: a review. J. Environ. Manag. 305, 114359. https://doi.org/10.1016/j.jenvman.2021.114359.

ASTM E1840-96, 2014. Standard Guide for Raman Shift Standards for Spectrometer Calibration.

Audy, P., Laroche, A., Saindon, G., Huang, H.C., Gilbertson, R.L., 1994. Detection of the bean common blight bacteria, *Xanthomonas campestris* pv. *phaseoli* and *X. c. phaseoli* var. *fuscans*, using the polymerase chain reaction. Phytopathology 84 (10), 1185–1192. https://doi.org/10.1094/phyto-84-1185.

Audy, P., Braat, C.E., Saindon, G., Huang, H.C., Laroche, A., 1996. A rapid and sensitive PCR-based assay for concurrent detection of bacteria causing common and halo blights in bean seed. Phytopathology 86, 361–366.

Baldi, P., La Porta, N., 2020. Molecular approaches for low-cost point-of-care pathogen detection in agriculture and forestry. Front. Plant Sci. 11, 570862. https://doi.org/10.3389/fpls.2020.570862.

Barzan, G., Sacco, A., Mandrile, L., Giovannozzi, A.M., Brown, J., Portesi, C., Alexander, M.R., Williams, P., Hardie, K.R., Rossi, A.M., 2020. New frontiers against antibiotic resistance: a Raman-based approach for rapid detection of bacterial susceptibility and biocide-induced antibiotic cross-tolerance. Sensor. Actuator. B Chem. 309, 127774.

Barzan, G., Kokalari, I., Gariglio, G., Ghibaudi, E., Devocelle, M., Monopoli, M.P., Sacco, A., Greco, A., Giovannozzi, A.M., Rossi, A.M., Fenoglio, I., 2022. Molecular aspects of the interaction with gram-negative and gram-positive bacteria of hydrothermal carbon nanoparticles associated with Bac8c2,5Leu antimicrobial peptide. ACS Omega 7 (19), 16402–16413. https://doi.org/10.1021/acsomega.2c00305.

Bräuer, B., Werner, M., Baurecht, D., Lieberzeit, P.A., 2022. Raman and scanning probe microscopy for differentiating surface imprints of *E. coli* and *B. cereus*. J. Mater. Chem. B 10 (35), 6758–6767. https://doi.org/10.1039/D2TB00283C.

Bull, C.T., et al., 2010. Comprehensive list of names of plant pathogenic bacteria, 1980–2007. J. Plant Pathol. 92, 551–592.

Bultreys, A., Kaluzna, M., 2010. Bacterial cankers caused by *Pseudomonas syringae* on stone fruit species with special emphasis on the pathovars *syringae* and *morsprunorum* race 1 and race 2. J. Plant Pathol. 92 (1 Suppl. l), S1.21–S1.33.

Cortes, C., Vapnik, V., 1995. Support-vector networks. Mach. Learn. 20, 273–297. https://doi.org/10.1007/BF00994018.

Cui, D., Kong, L., Wang, Y., Zhu, Y., Zhang, C., 2022. *In situ* identification of environmental microorganisms with Raman spectroscopy. Env. Sci. Ecotech. 11, 100187. https://doi.org/10.1016/j.ese.2022.100187.

de Siqueira e Oliveira, F.S.A., Da Silva, A.M., Pacheco, M.T.T., Giana, H.E., Silveira, L., 2020. Biochemical characterization of pathogenic bacterial species using Raman spectroscopy and discrimination model based on selected spectral features. Laser Med. Sci. 36, 289–302. https://doi.org/10.1007/s10103-020-03028-9.

Dragounová, K.A., Ryabchykov, O., Steinbach, D., Recla, V., Lindig, N., González Vázquez, M.J., Foller, S., Bauer, M., Bocklitz, T.W., Popp, J., Rödele, J., Neugebauer, U., 2023. Identification of bacteria in mixed infection from urinary tract of patient's samples using Raman analysis of dried droplets. Analyst 148, 3806–3816. https://doi.org/10.1039/D3AN00679D.

Eilers, P.H.C., Boelens, H.F.M., 2005. Baseline Correction with Asymmetric Least Squares Smoothing, 1.1. Leiden University Medical Centre Report, p. 5.

Fang, Y., Ramasamy, R.P., 2015. Current and prospective methods for plant disease detection. Biosensors 5 (3), 537–561. https://doi.org/10.3390/bios5030537.

FAO, 2020. www.fao.org/publications/card/en/c/CA7186EN.

Vanneste, J.L. (Ed.), 2000. Fire Blight: the Disease and its Causative Agent, *Erwinia Amylovora*. CABI, Wallingford, UK. http://www.cabi.org.

Franco-Duarte, R., Černáková, L., Kadam, S., Kaushik, K.S., Salehi, B., Bevilacqua, A., Corbo, M.R., Antolak, H., Dybka-Stępień, K., Leszczewicz, M., Relison Tintino, S., Alexandrino de Souza, V.C., Sharifi-Rad, J., Coutinho, H.D.M., Martins, N., Rodrigues, C.F., 2019. Advances in chemical and biological methods to identify microorganisms-from past to present. Microorganisms 7 (5), 130. https://doi.org/10.3390/microorganisms7050130.

Gallelli, A., Talocci, S., L'Aurora, A., Loreti, S., 2011. Detection of *Pseudomonas syringae* pv. *actinidiae*, causal agent of bacterial canker of kiwifruit, from symptomless fruits and twigs, and from pollen. Phytopathol. Mediterr. 50 (3), 462–472.

Geladi, P., MacDougall, D., Martens, H., 1985. Linearization and scatter-correction for near-infrared reflectance spectra of meat. Appl. Spectrosc. 39 (3), 491–500. https://doi.org/10.1366/0003702854248656.

Gomila, M., Busquets, A., Mulet, M., García-Valdés, E., Lalucat, J., 2017. Clarification of taxonomic status within the *Pseudomonas syringae* species group based on a phylogenomic analysis. Front. Microbiol. 8, 2422. https://doi.org/10.3389/fmicb.2017.02422.

Ho, C.S., Jean, N., Hogan, C.A., Blackmon, L., Jeffrey, S.S., Holodniy, M., Banaei, N., Saleh, A.A.E., Ermon, S., Dionne, J., 2019. Rapid identification of pathogenic bacteria using Raman spectroscopy and deep learning. Nat. Commun. 10, 4927. https://doi.org/10.1038/s41467-019-12898-9.

Huang, W.E., Li, M., Jarvis, R.M., Goodacre, R., Banwart, S.A., 2010. Shining light on the microbial world the application of Raman microspectroscopy. Adv. Appl. Microbiol. 70, 153–186.

Kałużna, M., Albuquerque, P., Tavares, F., Sobiczewski, P., Puławska, J., 2016. Development of SCAR markers for rapid and specific detection of *Pseudomonas syringae* pv. *morsprunorum* races 1 and 2, using conventional and real-time PCR. Appl. Microbiol. Biotechnol. 100 (8), 3693–3711. https://doi.org/10.1007/s00253-016-7295-0.

Koh, Y.J., Nou, I.S., 2002. DNA markers for identification of *Pseudomonas syringae* pv. *actinidiae*. Mol. Cells 13 (2), 309–314.

Kusić, D., Kampe, B., Ramoji, A., Neugebauer, U., Rösch, P., Popp, J., 2015. Raman spectroscopic differentiation of planktonic bacteria and biofilms. Anal. Bioanal. Chem. 407, 6803–6813. https://doi.org/10.1007/s00216-015-8851-7.

Lalucat, J., Gomila, M., Mulet, M., Zaruma, A., García-Valdés, E., 2022. Past, present and future of the boundaries of the *Pseudomonas* genus: proposal of *Stutzerimonas* gen. Nov. Syst. Appl. Microbiol. 45 (1), 126289. https://doi.org/10.1016/j.syapm.2021.126289.

Lane, D.J., 1991. 16S/23S rRNA sequencing. In: Stackebrandt, E., Goodfellow, M. (Eds.), Nucleic Acid Techniques in Bacterial Systematic. John Wiley and Sons, New York, pp. 115–175.

Lorenz, B., Wichmann, C., Stöckel, S., Rösch, P., Popp, J., 2017. Cultivation-free Raman spectroscopic investigations of bacteria. Trends Microbiol. 25, 413–424. https://doi.org/10.1016/j.tim.2017.01.002.

Lorenz, B., Rösch, P., Popp, J., 2019. Isolation matters—processing blood for Raman microspectroscopic identification of bacteria. Anal. Bioanal. Chem. 411, 5445. https://doi.org/10.1007/s00216-019-01918-8.

Lorenz, B., Guo, S., Raab, C., Leisching, P., Bocklitz, T., Rösch, P., Popp, J., 2022. Comparison of conventional and shifted excitation Raman difference spectroscopy for bacterial identification. J. Raman Spectrosc. 53, 1285. https://doi.org/10.1002/jrs.6360.

Lu, X., Al-Qadiri, H.M., Lin, M., Rasco, B.A., 2011. Application of mid-infrared and Raman spectroscopy to the study of bacteria. Food Bioprocess Technol. 4, 919–935.

Manoharan, R., Ghiamati, E., Dalterio, R.A., Britton, K.A., Nelson, W.H., Sperry, J.E., 1990. UV resonance Raman spectra of bacteria, bacterial spores, protoplasts and calcium dipicolinate. J. Microbiol. Methods 11. https://doi.org/10.1016/0167-7012(90)90042-5. I – 15.

Mansfield, J., Genin, S., Magori, S., Citovsky, V., Sriariyanum, M., Ronald, P., Dow, M., Verdier, V., Beer, S.V., Machado, M.A., Toth, I., Salmond, G., Foster, G.D., 2012. Top 10 plant pathogenic bacteria in molecular plant pathology. Mol. Plant Pathol. 13 (6), 614–629. https://doi.org/10.1111/j.1364-3703.2012.00804.x.

Mbega, E.R., Mabagala, R.B., Adriko, J., Lund, O.S., Wulff, E.G., Mortensen, C.N., 2012. Five species of xanthomonads associated with bacterial leaf spot symptoms in tomato from Tanzania. Plant Dis. 96, 760, 760.

Ogunlade, B., Tadesse, L.F., Li, H., Vu, N., Banaei, N., Barczak, A.K., Saleh, A.A.E., Prakash, M., Dionne, J.A., 2024. Rapid, antibiotic incubation-free determination of tuberculosis drug resistance using machine learning and Raman spectroscopy. Proc. Natl. Acad. Sci. U.S.A. 121, e2315670121. https://doi.org/10.1073/pnas.2315670121.

Pedregosa, F., Varoquaux, G., Gramfort, A., Michel, V., Thirion, B., Grisel, O., Blondel, M., Prettenhofer, P., Weiss, R., Dubourg, V., 2011. Scikit-learn: machine learning in Python. J. Machine Learning Research 12, 2825–2830.

PM 7/20 (3) *Erwinia amylovora*. EPPO Bull. 52, 2022, 198–224. https://doi.org/10.1111/epp.12826.

Powers, D., 2008. Evaluation: from precision, recall and F-factor to ROC, informedness, markedness & correlation. Mach. Learn. Technol. 2 (1), 37–63.

Prosen, D., Hatziloukas, E., Schaad, N.W., Panopoulos, N.J., 1993. Specific detection of *Pseudomonas syringae* pv. *phaseolicola* DNA in bean seed by polymerase chain reaction-based amplification of a phaseolotoxin gene region. Phytopathology 83, 965–970.

Ravatn, R., Zehnder, A.J., van der Meer, J.R., 1998. Low-frequency horizontal transfer of an element containing the chlorocatechol degradation genes from *Pseudomonas* sp. strain B13 to *Pseudomonas putida* F1 and to indigenous bacteria in laboratory-scale activated-sludge microcosms. Appl. Environ. Microbiol. 64 (6), 2126–2132. https://doi.org/10.1128/AEM.64.6.

Rebrošová, K., Šiler, M., Samek, O., Růžička, F., Bernatová, S., Holá, V., Ježek, J., Zemánek, P., Sokolová, J., Petráš, P., 2017. Rapid identification of staphylococci by Raman spectroscopy. Sci. Rep. 7 (1), 14846. https://doi.org/10.1038/s41598-017-13940-w.

Rebrosova, K., Samek, O., Kizovsky, M., Bernatova, S., Hola, V., Ruzicka, F., 2022. Raman spectroscopy—a novel method for identification and characterization of microbes on a single-cell level in clinical settings. Front. Cell. Infect. Microbiol. 12, 866463. https://doi.org/10.3389/fcimb.2022.866463.

Rees-George, J., Vanneste, J., Cornish, D.A., et al., 2010. Detection of Pseudomonas syringae pv. actinidiae using polymerase chain reaction (PCR) primers based on the 16S–23S rDNA intertranscribed spacer region and comparison with PCR primers based on other gene regions. Plant Pathol. (Oxf.) 59, 453–464.

Rodriguez, L., Zhang, Z., Wang, D., 2023. Recent advances of Raman spectroscopy for the analysis of bacteria. Anal Sci. Adv. 4, 81–95. https://doi.org/10.1002/ansa.202200066.

Ruokola, P., Dadu, E., Kazmertsuk, A., Häkkänen, H., Marjomäki, V., Ihalainen, J.A., 2014. Raman spectroscopic signatures of echovirus 1 Uncoating. J. Virol. 88, 8504–8513. https://doi.org/10.1128/JVI.03398-13.

Sacco, A., Portesi, C., Giovannozzi, A.M., Rossi, A.M., 2021. Graphene edge method for three-dimensional probing of Raman microscopes focal volumes. J. Raman Spectrosc. 52 (10), 1671.

Sampath, R., Hall, T., Massire, C., Li, F., Blyn, L., Eshoo, M., Hofstadler, S., Ecker, D., 2007. Rapid identification of emerging infectious agents using PCR and electrospray ionization mass spectrometry. Ann. N. Y. Acad. Sci. 1102, 109–120. https://doi.org/10.1196/annals.1408.008.

Satterfield, M.B., Marc, L., Salit, M.L., Choquette, S.J., 2008. Use of standard reference material 2242 (relative intensity correction standard for Raman spectroscopy) for microarray scanner qualification. Biotechniques 45 (2), 143–152. https://doi.org/10.2144/000112818.

Savary, S., Willocquet, L., Pethybridge, S.J., et al., 2019. The global burden of pathogens and pests on major food crops. Nat. Ecol. Evol. 3, 430–439. https://doi.org/10.1038/s41559-018-0793-y.

Scortichini, M., Marcelletti, S., Ferrante, P., Petriccione, M., Firrao, G., 2012. *Pseudomonas syringae* pv. *actinidiae*: a re-emerging, multi-faceted, pandemic pathogen. Mol. Plant Pathol. 13 (7), 631–640. https://doi.org/10.1111/j.1364-3703.2012.00788.x.

Sorensen, K.N., Kim, K.H., Takemoto, J.Y., 1998. PCR detection of cyclic lipodepsinonapeptide-producing *Pseudomonas syringae* pv. *syringae* and similarity of strains. Appl. Environ. Microbiol. 64 (1), 226–230. https://doi.org/10.1128/AEM.64.1.226-230.1998.

Stöckel, S., Kirchho, J., Neugebauer, U., Rösch, P., Popp, J., 2016. The application of Raman spectroscopy for the detection and identification of microorganisms. J. Raman Spectrosc. 47, 89–109. https://doi.org/10.1002/jrs.4844.

Thomsen, B.L., Christensen, J.B., Rodenko, O., Usenov, I., Grønnemose, R.B., Andersen, T.E., Lassen, M., 2022. Accurate and fast identification of minimally prepared bacteria phenotypes using Raman spectroscopy assisted by machine learning. Sci. Rep. 12 (1), 16436. https://doi.org/10.1038/s41598-022-20850-z.

Tu, Q., Chang, C., 2012. Diagnostic applications of Raman spectroscopy. Nanomed. Nanotechnol. Biol. Med. 8, 545–558.

Turano, T.A., Hartman, K.A., Thomas, G.J., 1976. Studies of virus structure by laser-Raman spectroscopy. 3. Turnip yellow mosaic virus. J. Phys. Chem. 80, 1157–1163. https://doi.org/10.1021/j100552a008.

Vanneste, J.L., 2017. The scientific, economic, and social impacts of the New Zealand outbreak of bacterial canker of kiwifruit (*Pseudomonas syringae* pv. *actinidiae*). Annu. Rev. Phytopathol. 55, 377–399. https://doi.org/10.1146/annurev-phyto-080516-035530.

Venbrux, M., Crauwels, S., Rediers, H., 2023. Current and emerging trends in techniques for plant pathogen detection. Front. Plant Sci. 14, 1120968. https://doi.org/10.3389/fpls.2023.1120968.

Wold, S., Sjöström, M., Eriksson, L., 2001. PLS-regression: a basic tool of chemometrics. Chemometr. Intell. Lab. Syst. 58 (2), 109–130.